HOW TO FIND A ROOT: MODELING AND MICROFLUIDIC PLATFORMS DEVELOPED FOR INVESTIGATION OF NON-CANONICAL SMALL MOLECULE C-DI-GMP'S ROLE IN CHEMOTAXIS OF *AZOSPIRILLUM BRASILENSE*

By

Alexander Aaring

A THESIS

Submitted to
Michigan State University
in partial fulfillment of the requirements
for the degree of

Microbiology and Molecular Genetics – Master of Science

2023

ABSTRACT

Chemotactic bacteria explore their environments and bias their travel towards attractive gradients and away from repellant gradients. Plant root microbiomes are enriched for bacteria with chemotaxis genes, and soil microbes have more complex chemotactic machinery than model systems like E. coli. The temporal, chemical, and spatial complexity of soil likely necessitates nuance for chemotaxis. Model cereal crop-associated bacterium Azospirillum brasilense has c-di-GMP binding domains on several of its chemoreceptors, and under laboratory conditions, c-di-GMP plays a role in modulating chemotaxis. To investigate how c-di-GMP modifies chemotactic signal transduction in this agriculturally important species, we developed agent-based computational models and novel microfluidic device designs and methods.

TABLE OF CONTENTS

CHAPTER 1: INTRODUCTION

Global pressures on growing conditions for crops threaten food and economic security[1]. Largest among these is climate change, which is changing the growing of all plants and leaving some areas no longer suitable for crops[1]. Combined with increasing demand from population growth, the need for technological advancements in crop security is high[1]. Historically we have relied on chemical fertilizers to improve crop yields, but the high cost, reduced availability, and greenhouse gas emissions associated with the production and use of chemical fertilizers has led to an increase in interest in so-called “green fertilizers”, which are microbial soil amendments[1,2].

The science behind green fertilizers starts with the observation that the rhizosphere (root associated) microbial community has the capacity to improve growth rates, crop yields, and stress resistance, including resistance against potential pathogens, heat, and drought stresses[1,2]. Commonly bacterial members of healthy rhizosphere communities will colonize the surface of roots and provide various benefits, such as producing plant growth promoting hormones that improve the yield of the crop[1–3].

To maximize green fertilizer effectiveness, it is important to understand both which microbes promote plant growth and health and how those microbes are recruited to the root surface. To answer the latter, we start with the question: are rhizosphere communities actively attracted to the roots or do roots rely on random encounters and immune systems to select only beneficial microbes? Evidence suggests the former as from metagenomic studies it has been observed that rhizosphere bacterial communities are enriched for chemotaxis pathways relative to bulk soil bacterial communities[4]. These observations have been supported by *in vitro* studies showing that rhizosphere associated bacterium *Azospirillum brasilense* will swim towards roots[5].

The observation that many of the members of rhizosphere communities chemotax to the root raises a new question: with soil being chemically and physically complicated compared to other systems[2,6], how are these bacteria adapted to navigating in soil? Chemotaxis is one of the most well-studied post-translational signaling pathways[7,8]. With flagellar swimming motility, bacterial cells explore their environment via a random walk behavior, alternating between relatively straight runs and reorienting tumbles (or reversals in the case of monoflagellates)[7,9].

Chemotaxis signaling biases the random walk in response to bound ligand, leading cells to travel up attractive gradients and down repellent gradients on average across a population[7,8].

The most well studied bacterial chemotaxis system is *E. coli. E. coli* was initially studied because tools for general propagation and genetic manipulation were developed for E. coli

before many other organisms. The general architecture of the chemotaxis signaling pathway is expected to be conserved across species of bacteria.

To explain the *E. coli* chemotaxis pathway briefly, chemoreceptors form hetero-trimers of homo-dimers based on the length of a spacer region that forms an alpha helix in all receptors[7]. Chemoreceptors associate with other receptors that have spacer loops of the same length[7]. The chemoreceptor hexamers form larger arrays, mostly in the cell membrane, though some receptors are cytosolic like Aer, the oxygen sensing receptor[7]. Hexamers are associated with CheA, sometimes through the adapter protein CheW[7]. CheA has autophosphorylation activity and will pass a phosphate group to CheY or CheB[7]. CheY-P interacts with the motor complex and causes the flagella to switch from counterclockwise rotation to clockwise rotation, functionally causing the cell to stop swimming forward ("running") and randomly reorient instead ("tumbling")[7]. CheY-P is dephosphorylated at a constant rate by CheZ[7]. When chemoreceptors bind to an attractant, they inhibit the autophosphorylation activity of CheA, leading to less CheY-P and more running behavior[7]. To capture some memory of past concentrations and adapt the sensation of environmental signal, the chemoreceptors are methylated at a constant rate by CheR and dephosphorylated by CheB-P[7]. Chemoreceptor cluster inhibition of CheA autophosphorylation is reduced by methylation[7] (figure 1.1).

Compared to *E. coli*'s 5 canonical chemoreceptors and single chemotaxis operon, soil microbes often have dozens of chemoreceptors and multiple chemotaxis operons with redundant gene annotations[10]. Using the basis of *E. coli*'s well-studied system, we investigated how a representative soil microbe's chemotaxis signaling pathway is different to find out how it is adapted to soil.

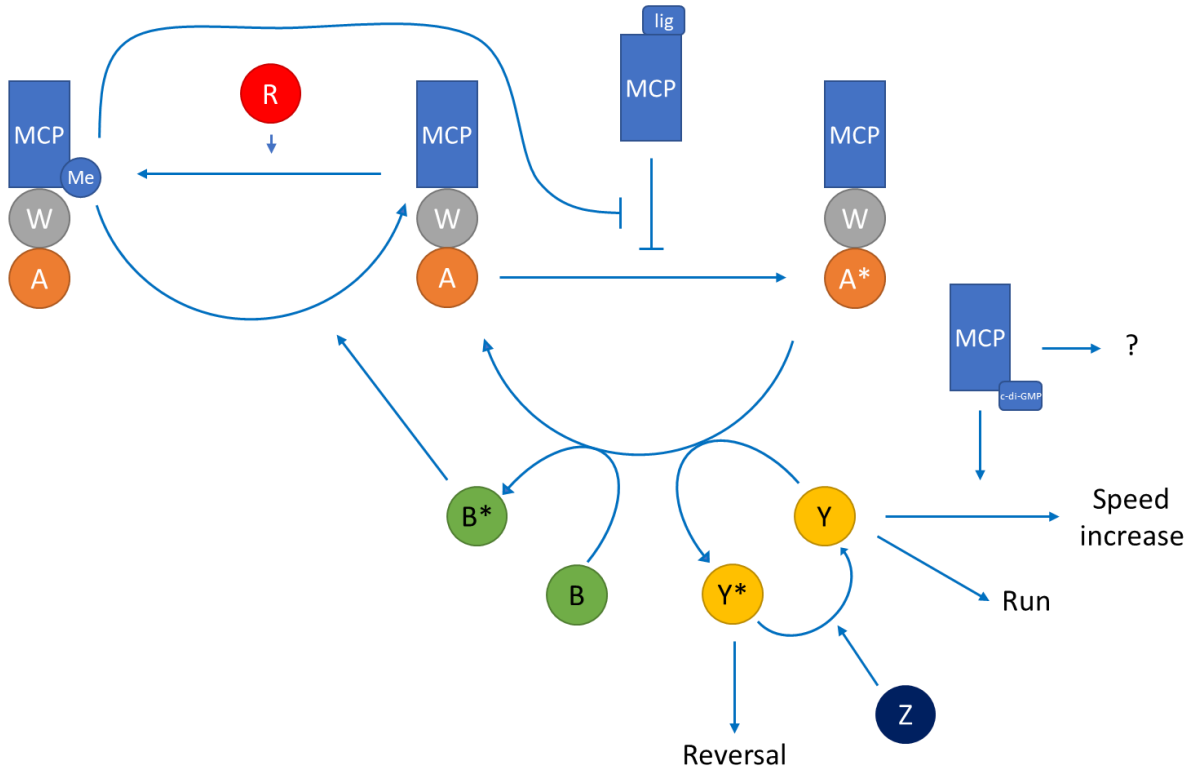

Figure 1.1. Simplified chemotaxis signal transduction pathway in A. brasilense. Methyl-accepting chemoreceptor proteins (MCPs) raft together in the membrane as hexamers of homodimers. These clusters bind to CheW which links them to CheA. CheA has autophosphorylation activity and will then pass its phosphate group to CheY or to CheB. CheY-P (Y*) binds to the flagellar motor and promotes the switch from CCW rotation to CW rotation. In polyflagellated cells, this is the transition from Run to Tumble, and in monoflagellates like *A. brasilense* it is Reversal. CheY-P is dephosphorylated at a constant rate by CheZ. When an MCP binds an attractant ligand, it inhibits the autophosphorylation of CheA, resulting in a lower proportion of CheY-P:CheYTot and more forward swimming. MCPs are also methylated at a constant rate by CheR. Methylated MCPs have less inhibitory activity when bound to ligand than unmethylated MCPs, making the pathway effectively less sensitive to ligand as the receptors are methylated. This is kept in balance by CheB-P (B*) which demethylates MCPs. In *A. brasilense* c-di-GMP also binds MCPs and may be associated with an increase in swimming speed transiently as well as other impacts.

Azospirillum brasilense and non-canonical signaling

Azospillum brasilense is plant growth promoting bacterium that associates generally with the roots of cereal grains and is the most common bacterial component of green fertilizers[1,11]. *A. brasilense* is a microaerophilic nitrogen fixing bacterium but does not appear to share fixed

nitrogen with plant hosts[11]. Instead, it promotes the growth of the plant by producing plant growth hormones[11]. While capable of nitrogen fixation, *A. brasilense* will preferentially grow on labile nitrogen and under those conditions grows well aerobically[12]. Soil systems can have high temporal heterogeneity with regards to access to water and other nutrients and *A. brasilense* manages this uncertainty by forming cysts in times of resource shortage and storing energy and carbon in the form of poly-β-hydroxy-butyrate granules within the cell[13–15].

It has 4 chemotaxis operons as well as other chemotaxis genes outside these operons and about 50 annotated chemoreceptor genes[10]. Of these operons, 2 are expressed under laboratory conditions, 1 is not expressed, and the last is involved in cyst formation instead of chemotaxis[16]. Among the chemotaxis genes, there is a significant amount of apparent redundancy. While there are at least 4 copies of each CheA and the adaptor protein CheW, these appear to associate interchangeably with each other and the chemoreceptor clusters[17]. *A. brasilense* also has 7 copies of CheY and one study has suggested that these may have minor differences in their downstream activity[10]. Genes annotated as copies of CheB and CheR are encoded in *A. brasilense,* and the chemoreceptors have potential methyl-accepting domains, but methylation has not yet been validated in *A. brasilense*. That said, knock-out strains for CheB and CheR alter the ability of *A. brasilense* to perform chemotaxis in the standard capillary band formation assay[18], so they are likely active. The chemoreceptors themselves form 3 distinct clusters in the cell: 2 embedded in the membrane that differentiate based on the length of the repeat loop[17], and a third group that is soluble in the cytoplasm[5]. *A. brasilense* expresses different numbers of flagella depending on its current lifestyle[19]. When swimming, it is a polar monoflagellated and this is the state in which its chemotaxis has been studied[12]. *A. brasilense* can also express flagella peritrichously like *E. coli*, but this appears to be for the purpose of surface attachment rather than motility[19].

A. brasilense has been shown to chemotax to the surface of roots *in vitro*[5]. Chemoreceptors that are sensitive to organic compounds that have been investigated in *A. brasilense* have shown promiscuous binding to a wide array of root exudates and similar compounds[20]. This is consistent with the *in situ* observation that *A. brasilense* associates generally with the roots of plants rather than forming highly specific associations[11]. Another interesting observation about *A. brasilense*'s chemotaxis phenotype is that it performs precision energy taxis: in an attractive gradient, A. brasilense will create a band of higher cell concentration at an optimum attractant concentration based on the redox state of the attractant and the redox potential inside the cellsruss[5,18,20–25]. This band formation phenotype underlies the standard assays that have been used to study *A. brasilense*'s chemotaxis for decades[12].

One of the most interesting differences between *A. brasilense*'s chemotaxis machinery and *E. coli*'s is that several of the chemoreceptors have PilZ domains that have been shown to bind cyclic-di-guanylate-monophosphate (c-di-GMP)[5,20,26]. Incorporation of non-canonical signals like the small molecule second messenger c-di-GMP into chemotaxis and other pathways is more common outside of the domesticated lab strains[27–29]. C-di-GMP is produced by diguanylate cyclases (DGCs) from 2 GTP molecules and so is produced more when energy is more available in the cell[29]. It also has a short lifespan in the cell before being broken down by phosphodiesterases (PDEs), so production and breakdown is likely specific to different regional microenvironments in the cell[29]. As a signal of high energy availability, it is perhaps unsurprising that c-di-GMP is mostly associated with the transition from motile to sessile lifestyles and the production of biofilms[29]. That said, recent research has shown that c-di-GMP signaling has a wide diversity of targets and outcomes[29], such as in *E. coli* where YcgR with bound c-di-GMP acts as a brake on the flagellar motor[30]. In *A. brasilense*, extended elevation of [c-di-GMP] does lead to a transition from motile to sessile but has also been associated with a transient increase in swimming speed[20]. Altering or removing c-di-GMP binding domains from chemoreceptors has been shown to alter band formation behavior in chemotaxis assays[20].

All these attributes make *A. brasilense* a good candidate for further work as a model system. It is like *E. coli* in the general architecture of the chemotaxis pathway[31], providing a basis for investigating the specific aspects that are different, such as the inclusion of c-di-GMP binding domains in several chemoreceptors.

Question of the thesis

In the present work we focused on investigating the role of c-di-GMP in the chemotaxis pathway of *A. brasilense*. This was chosen both because it is a unique aspect of the *A. brasilense* pathway compared to the *E. coli* model and because outside the *A. brasilense* system the role of non-canonical small molecule messengers is understudied. It is expected that c-di-GMP binding to select chemoreceptors provides the feedback mechanism that allows *A. brasilense* cells to be responsive to both the external environment and to their own internal redox state. This was expected to occur via allosteric changes to the affected chemoreceptors resulting in altered downstream signaling.

How to answer the question

There are many ways that c-di-GMP binding could result in the observed chemotaxis phenotypes biochemically, enough that generating every necessary mutant and running the existing assays would more time and resources than are available. To answer the question, we

settled on two main methodologies. Since the interactions of enzymes and substrates in a cell can be described by mathematical equations, we first aimed to use computational models to solve numerically for the chemotaxis behavior of *A. brasilense* based on published data. With many moving parts, it was expected that there would be more than one model that was consistent with past data. These models would then be used to predict chemotaxis behavior under novel conditions to find conditions predicted to discriminate between the models. Second, custom microfluidic devices were created and used to generate environmental conditions predicted to discriminate between potential biochemical models. The computational models would then be refined based on the microfluidic data.

Computational modeling to generate hypotheses

Computational modeling is an efficient way to explore potential logical interactions in a system that is well developed. There are two main approaches to computational models for chemotaxis. To simplify, there is the approach that focuses on population average performance (mean field theory) and there is the agent-based approach that keeps track of all individuals. For the present work we chose to use agent-based modeling for cells because we are interested in root colonization, which can be done by a minority of cells in a population, rather than in the average behavior. The internal biochemistry uses a mean field approach because the motions of individual proteins in the system is more resolution than is required. There is good evidence that phenotypic diversity in isogenic populations will lead to outliers sometimes being high performing in chemotaxis[32]. We would be losing important data if we only looked at the average in this case.

Both mean field theory and agent-based modeling are well developed in *E. coli*[32–36]. As *A. brasilense*'s chemotaxis pathway looks fairly similar to *E. coli*'s pathway[31], we were able to use past work as a foundation for our modeling. Mean field theory work in *E. coli* is the basis for a significant amount of theory about how microbes explore and navigate in their environment. From this work we can also take a starting understanding of how cells can perform precision taxis: (1) one receptor senses a signal as attractive while a different receptor senses the same signal as repellent; (2) a single receptor changes whether it senses a signal as attractive or repellent based on the concentration of the signal (as it pH taxis); or (3) a single receptor alters its affinity for a different ligand based on the concentration of signal in the gradient (as in thermotaxis)[36]. The other way to achieve band formation is to have two different overlapping gradients with distinct receptors pulling cells in different directions.

In our work we adapted prior models to fit the case of *A. brasilense*. We changed the way that agent-cells in the system adjust their direction in 3-D by modeling directional change during a

tumble in the same way as changes due to Brownian forces with a larger magnitude[37]. We also added in terms for testing the role of c-di-GMP and found that our model behaved qualitatively as expected based on published literature. This agent-based modeling approach has been shown in *E. coli* to replicate *in vivo* behavior of bacterial populations more accurately[32,33]. Because the specific biochemical and environmental differences in the chemotaxis pathway of soil microbes is not well understood, the additional detail provided by modeling the cells as individual agents will provide a better understanding of how c-di-GMP interacts with chemotaxis machinery to produce precision taxis behavior in *A. brasilense*.

Microfluidics to validate models

To test and refine the computational modeling predictions it was necessary for us to create chemical and physical environments with a high degree of control. Microfluidics has been used for decades to create systems with physical features on scales that are meaningful to individual cells[38–41]. In our work this process was used to create chambers for observing motility and chemotaxis phenotypes, but microfluidics has also been used to study growth, morphology, and chemical reactions, among other topics.

Past work into mimicking soil systems with microfluidics has focused on physical obstacles and convolution[42]. Some pore spaces in soil are very restricted in bacterial terms, to the point where the pore spaces have widths that are on the order of the width of cells[43]. When bacteria are challenged with highly restricted spaces like that, the ability to change direction is restricted directly by the walls of the environment so cells that try to change direction less frequently explore the space more quickly[43]. In our work we did preliminary tests using a webapp model (https://dufour.mmg.msu.edu/chemotaxisApp/chemotaxis.html) to see if these or any physical obstacles changed optimal adaptation of chemotaxis enzyme activities. We were unable to find any other physical obstacles that led to differences in the optimal enzyme activities to traverse obstacles and reach an attractant source (figure 1.2). This is in line with literature suggesting that evenly spaced obstacles have no impact on chemotactic performance[44].

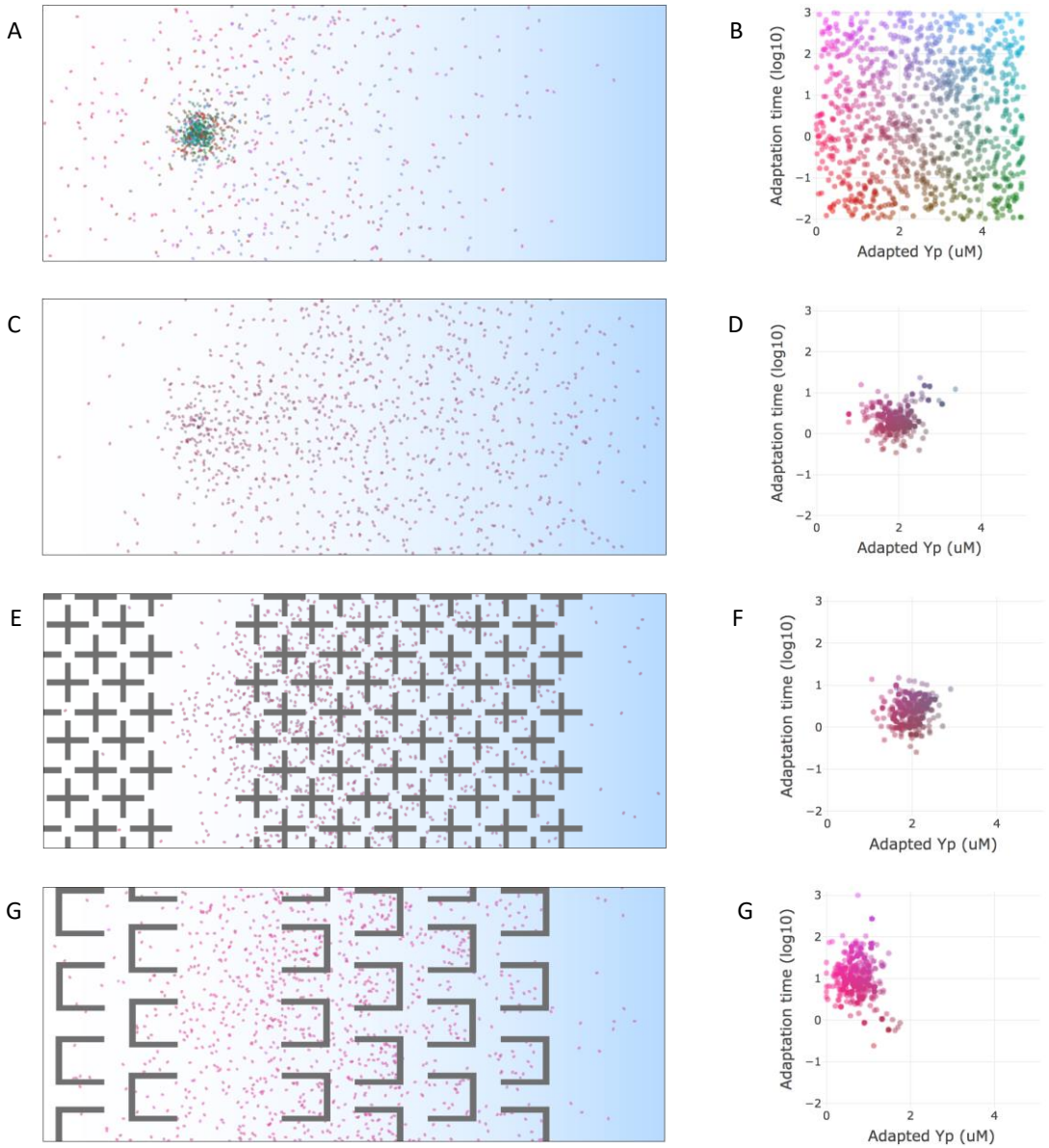

Figure 1.2. Webapp model results suggest that evenly spaced regular obstacles do not require different adaptation than open space while "ratchet" style obstacles do require different adaptation. (A) At the beginning of the model cells are in an open 2-D space with an attractive gradient. (B) These cells are randomly distributed in phenotype across two parameters: Adapted Yp relates to the relative amount of CheY-P in the cell and the Adaptation time relates to the rate of methylation. (C,D) With the "Evolve" option on, as cells reach the source end of the gradient, both that cell and another cell chosen at random are removed and two new cells with parameters close to the cell that reached the goal are spawned at the start location. Over time this leads to a simple simulation of evolutionary adaptation. (E,F) The system was let to "evolve" with relatively dense regular obstacles. The optimal evolutionary

Figure 1.2 (cont'd)
adaptation under these conditions was found to be the same as it was for the no obstacle case. However, when challenged with "ratchet" style obstacles that require the cells to swim towards lower concentrations of attractant sometimes to avoid being trapped these cells perform poorly. (G,H) Instead, when let to evolve with trap/ratchet obstacles, the optimal evolutionary adaptation is to be less sensitive to the gradient and more explorative.

Soil is also chemically complicated and controlling the chemical environment was key to testing hypotheses generated by the modeling, but devices to create non-linear or overlapping gradients are uncommon. Glass is not permeable to attractants over relevant timescales and PDMS is only permeable to non-polar compounds and gases. The most relevant attractants are root exudates[5,45], which are polar compounds that are often sugar derivatives, so they do not pass through PDMS walls. The most common way to set up a gradient is some variant on making two chambers connected with a bridge region. Each chamber is filled with a different concentration of chemoattractant and a gradient is formed in the bridge[46]. The gradient in this case though stabilizes as a linear gradient[46]. Another method is to create separated chambers and either use an attractant that passes through PDMS like oxygen[47] or to use a hydrogel for the wall[40,48–51]. This separated chamber style as the advantage that the other chambers in the system can be set up as flow channels, effectively making those chambers unchanging in concentration. However, this method has only been used to create single, linear gradient systems[40]. An in-between approach has also been used wherein a device is designed with mostly separated chambers except for micro-slits that allow for diffusion but limit flow[52].

In our work we combine the design principles of separated chambers with hydrogel walls with the ability to graft polyethylene glycol (PEG) onto PDMS and create a hybrid material device[53]. By using diffusion modeling we found that holding the edges of a central chamber at constant concentrations could generate non-linear gradients. We can hold those edges at constant concentrations by creating flow channels separated from the central chamber by hydrogel walls. We showed that the design effectively creates overlapping exponential gradients. However, we also struggled with the delicacy of the system as the PEG-glass interface in the devices is not covalently linked in the same way that the PDMS-glass interface is.

CHAPTER 2: COMPUTATIONAL MODELING OF THE ROLE OF C-DI-GMP IN *A. BRASILENSE* PRECISION TAXIS BAND FORMATION BEHAVIOR

Introduction

Plant rhizosphere bacterial communities are enriched for bacteria with chemotaxis genes[4], and these pathways have key differences from the lab model, *E. coli*[10]. For our work we used *A. brasilense* as a representative rhizosphere microbe. In general, the *A. brasilense* chemotaxis pathway is like *E. coli*'s[31], but importantly it has been shown that several of the chemoreceptors also bind c-di-GMP and that this binding alters the chemotactic behavior of the cells[5,20,26]. This may explain one of *A. brasilense*'s unusual behaviors *in vitro*: *A. brasilense* performs precision energy taxis, meaning that populations will congregate at specific concentrations of attractants based on their redox state and the internal redox state of the cell[5,18,20–23,25,26]. It is hypothesized that c-di-GMP activity may be the chemical signal that *A. brasilense* senses as a measure of internal redox state of the cell, and in this role c-di-GMP contributes to the precision energy taxis phenotype.

C-di-GMP is a small molecule secondary messenger that has been characterized for its role in the transition from motile to sessile lifestyles and the formation of biofilms[29,54]. In *A. brasilense*, elevated c-di-GMP levels also signals for the transition from motile to sessile over transcriptionally relevant time scales, and at shorter time scales it also is involved in apparent increases in swimming speed as well as precision taxis band formation[20]. The current evidence suggests that c-di-GMP alters chemotactic behavior, such as swimming speed and preferred concentration for precision energy taxis band formation, through binding to the chemoreceptors[20,26]. Unfortunately, c-di-GMP is a short-lived molecule and has highly localized production, sensation, and degradation in the cell, making it difficult to measure real time changes in the internal activity of c-di-GMP[29]. In this work we seek to answer how c-di-GMP activity is incorporated into the chemotaxis signal transduction pathway. Doing so will shed light on how non-canonical signals are incorporated into chemotaxis, which has implications for any system where bacterial chemotaxis is important.

There are many ways that c-di-GMP binding to chemoreceptors could result in changes to the chemotaxis of the cells. Generating all the mutants necessary to test all the possibilities would likely not be completable with the resources and time available. However, the interactions in the chemotaxis pathway are logical and can be represented mathematically. We can use

mathematical models to computationally test a wide variety of different possibilities efficiently and determine which of the interactions is consistent with current data quantitatively and what experimental conditions can be used to discriminate between the possibilities.

Computational models for chemotaxis in *E. coli* are well-developed, both for determining mean chemotactic behavior in a population and for determining the individual behavior of cells[32–36]. Usefully, these models include some ways that precision taxis can occur: two separate and opposed gradients; one gradient that is attractive to one receptor and repellent to another receptor; or one gradient that is either attractive or repellent to the sensitive receptor depending on the concentration of the ligand[36].

In the work described, we adapted the agent-based *E. coli* chemotaxis models to *A. brasilense*. To investigate the role of c-di-GMP in the precision energy taxis of *A. brasilense*, we added c-di-GMP activity as a multiplier on factors expected to be directly changed as a result of c-di-GMP binding, that is to say the relative free energy of different chemoreceptor confirmations as represented in our model. We then examined how the band formation behavior changed as a function of changing the activity of c-di-GMP. In published work on *A. brasilense* chemotaxis, metrics that have been used to measure the bands include the position of the band relative to the gradient, how long the band takes to form and equilibrate, and the width of the band[5,12,18,20–26]. To make sure that our models are accurately replicating *in vitro* data, we need to measure the same traits of the band as published literature. To analyze the resulting bands, we employed cumulative density and looked at the median point of the density as a measure of band position and the slope at the median. Based on our model, we expected a loss of band formation activity at high c-di-GMP activity for most of the factors tested as well as a loss of band formation at low c-di-GMP activity for receptor active energy (the relative free energy of the receptor in the confirmation that actively inhibits CheA autophosphorylation). Our results matched our predictions and serve as a successful proof of principle for the computation modeling as a means of interrogating the system and provides a basis to build additional complexity in looking at soil bacterial chemotaxis as well as chemotaxis in other systems.

Materials & Methods

The code for this work, pyBacKinesis, can be found on GitLab (https://gitlab.msu.edu/dufourlab/pybackinesis). The model presented here is a translation of and expansion on the model published in Frankel NW, et al, 2014[33]. In brief, these are agent-based mass action models based on the Monod-Wyman-Changeux model. Chemotaxis behavior is a function of the rate at which the cells switch between forward “run” movement and reorienting “tumbles” for polyflagellates or “reversals” for monoflagellates. This rate is a function

of the proportion of phosphorylated CheY (CheY-P) to total CheY ($CheY_{Tot}$), which in turn is a function of the activity of CheA (*a*). CheA activity is a function of the concentration of ligand ($f_L(\mathbf{L})$) and the average methylation state of the chemoreceptors ($f_m(m)$) scaled by the cooperativity constant of the receptor cluster (N_{coop}) and follows the form of a Hill equation (eq 1).

$$a(m, \mathbf{L}) = \left[1 + exp\left(N_{coop}(f_m(m) + f_L(\mathbf{L}))\right)\right]^{-1} \quad (1)$$

The contribution of the each ligand concentration (**L**) is determined by the relative population of each receptor (**r**) and the constants of association ($\mathbf{K_{on}}$) and dissociation ($\mathbf{K_{off}}$) for each receptor with each ligand (eq 2). Each of these values is a vector.

$$f_L(\mathbf{L}) = \mathbf{r} \ln\left[\frac{1 + \mathbf{L}/\mathbf{K_{off}}}{1 + \mathbf{L}/\mathbf{K_{on}}}\right] \quad (2)$$

The contribution of the methylation state is linear and determined by the difference between the current average methylation state (m_c) and the baseline average methylation state when there is no ligand (m_0) scaled by a experimentally determined constant (E_m) (eq 3).

$$f_m(m) = -E_m(m_c - m_0) \quad (3)$$

At any given ligand concentration there is an adapted average methylation state (m_a) that the cell will approach over time. The adapted average methylation state can be calculated as the difference between $f_L(\mathbf{L})$ scaled by N_{coop} and the relative free energy of the active enzyme complex with ligand bound (T_{active}) and m_0 (eq 4). We calculate m_c numerically by first calculating the change in methylation with respect to time at the current time (eq 5), interpolating to the next time step in the simulation, then repeating. Methylation is much slower than other reaction rates in the system, so as long as the time steps of the simulation (we used 0.001 s steps) are much faster than the time scale relevant for methylation to occur (around 0.5 to 1 s in *E. coli*) this simulation will accurately represent the behavior of the individual cells. Eq 5 also includes a noise term $\eta_m(t)$ to capture the entropically determined randomness in biochemical interactions in the system.

$$m_a(\mathbf{L}) = m_0 - \left(\frac{N_{coop}}{\mathbf{T_{active}}}\right) f_L(\mathbf{L})$$
$$= m_0 - \left(\frac{N_{coop}}{\boldsymbol{T_{active}}}\right) \boldsymbol{r}\, ln\left[\frac{1 + {\boldsymbol{L}}/{\boldsymbol{K^{off}}}}{1 + {\boldsymbol{L}}/{\boldsymbol{K^{on}}}}\right] \quad (4)$$

$$\frac{dm}{dt} = -\frac{1}{\tau}\left(m_c - m_0(\mathbf{L})\right) + \eta_m(t) \quad (5)$$

By restating eq 1 in terms of T_{active} and the free energy of the inactive enzyme complex with ligand bound ($T_{inactive}$) using the relationship in eq 6, we get eq 7.

$$N_{coop}(f_m(m) + f_L(\boldsymbol{L})) = \mathbf{r}[\mathbf{T_{inactive}} + \mathbf{T_{active}}(m_0 + m_c - m_a)] \quad (6)$$

$$a(m, \mathbf{L}) = [1 + exp(\mathbf{r}[\mathbf{T_{inactive}} + \mathbf{T_{active}}(m_0 + m_c - m_a)])]^{-1} \quad (7)$$

As there is biochemical evidence that c-di-GMP binds directly to chemoreceptors and this binding changes the signal transduction[20,26], we initially tested whether c-di-GMP was a direct modifier of one of the factors physically associated with the chemoreceptors. We chose factors expected to effected by conformational changes in the receptor as a result of c-di-GMP binding: the stability of the ligand bound, ligand unbound, active, and inactive states of the chemoreceptors, and the cooperativity between receptors in a cluster. For each of these, c-di-GMP activity was added as a direct multiplier in the model and then the c-di-GMP activity was varied exponentially from 2^{-10} to 2^{10} to cover a wide range of conditions. There are not currently published data regarding the local concentration range of c-di-GMP at the chemoreceptor arrays across different conditions of interest or how those concentrations are converted to activities in the chemotaxis pathway. However, those are not necessary to investigate the role of c-di-GMP in the system computationally as the concentration is abstracted to an activity measure anyway and there is published data using optogenetic phosphodiesterase (c-di-GMP depletion) and

diguanylate cyclase (c-di-GMP production) strains of *A. brasilense* that provide a qualitative understanding of how changes in c-di-GMP concentration affects band formation in a gradient[26]. *A. brasilense* forms bands in gradients[12], so to run initial tests an opposed gradient system was used to ensure that a band formed. Specifically opposed sigmoidal curves following the form of the Boltzmann equation were used. The Boltzmann equation itself is not thought to be meaningful in this context, but exponential and sigmoidal gradients are transiently observed in nature and are convenient for modeling.

That said, in our computational models we have perfect information about the position of every cell at every point in time, so we can be more quantitative than *in vitro* assays. We employed cumulative density plots as a means of analyzing our bands. The median point of the cumulative sum works as a proxy for the position of the band and the slope at the median point is a robust metric for measuring the sharpness of the band. “Sharpness” here is a measure of the relative density of cells around the middle of the band compared to the density away from the band. In a cumulative density plot the slope increases more rapidly in regions of higher density, so at any given point the slope can be considered a measure of the density at that point. By measuring and comparing the median and slope at the median across time in the simulation we can compare to the published metrics, including when the band equilibrates.

Results

Band formation

As a baseline for generating a band, we used a pair of opposed sigmoidal gradients. This creates an energetically optimal region in the middle of the system where the cells are predicted to congregate. When we ran simulations in this system, the modeled cells formed a band of higher cell density in this region as predicted (figure 2.1).

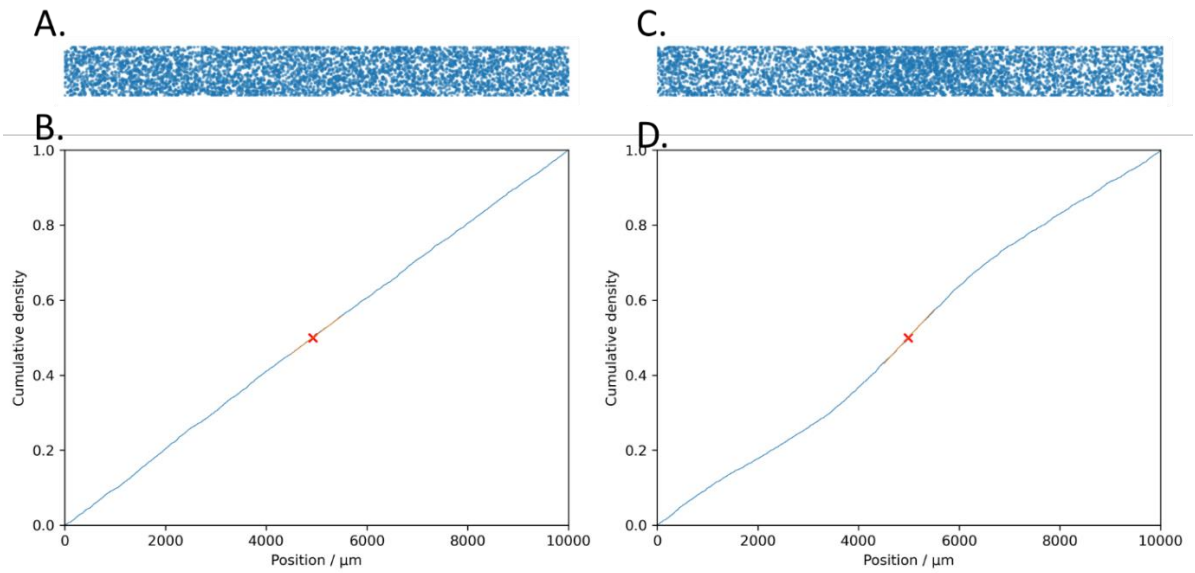

Figure 2.1. Band formation in agent-based model quantified using cumulative sum plots. (A) Initial cell positions uniformly distributed. (B) This is reflected in the cumulative sum plot, which shows a constant increase in cumulative density over the x-axis. (C) At the end of the simulation, cells have congregated in the middle of the chamber. (D) In the cumulative sum plot this is reflected by the sharper increase in the density at the middle compared to the edges, resulting in an S-shaped plot. The median cell is denoted by the red “x” in the cumulative sum plots as a measurement of the band position. The orange lines are the slope of the line around the median and is a measure of the “sharpness” of the band.

Impact of c-di-GMP on the model

C-di-GMP was included in the model as a multiplier of several different elements and then varied across powers of 2. The band formation results match the qualitative predictions (figure 2.2). The effect of c-di-GMP was added symmetrically across different receptors in the model for these trials, so as expected the position of the band did not change as measured by the median of the cumulative density plot.

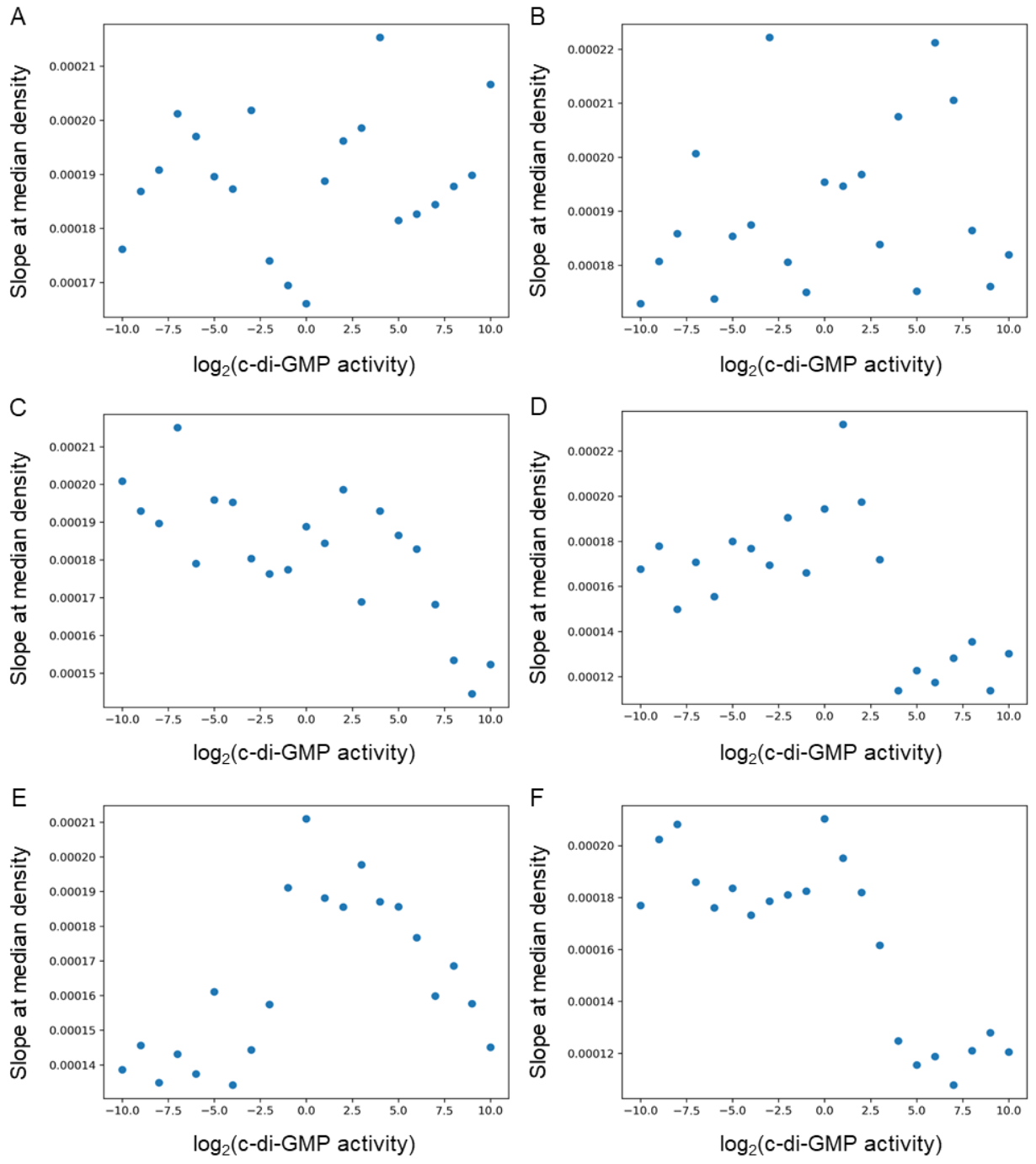

Figure 2.2. Scatter plots of the slope at median density of the cumulative density plot vs log2(c-di-GMP activity). Each plot represents a different aspect of the computational model that was associated with c-di-GMP activity for that trial. Each point represents the slope at the median of the cumulative density plot after a single run with 5000 simulated cells until the band equilibrated (1800 s). (A) Control: When c-di-GMP activity is varied without being associated with any part of the model equations, the sharpness of the band varies randomly. (B) Ligand

Figure 2.2 (cont'd)
association constant: When the receptor-ligand association constant is associated with c-di-GMP activity, the band sharpness varies randomly. (C) Ligand dissociation constant: associating the receptor-ligand dissociation constant with c-di-GMP activity leads to a loss of the band with increasing c-di-GMP activity. (D) Receptor cooperativity: receptor cooperativity makes no difference to the band sharpness at low c-di-GMP activity and fails to form a band at high c-di-GMP activity. (E) Receptor active energy: when log(c-di-GMP activity) is near zero and therefore having the least effect is when the band is sharpest. As c-di-GMP increases or decreases away from that, the band fails to form. (F) Receptor inactive energy: similar to the dissociation constant and the cooperativity constant, when the energy level of the inactive receptor is associated with c-di-GMP activity there is little to no change as the activity approaches zero and a loss of band formation when the activity starts to increase.

Discussion

The work presented here matches qualitative expectations and expands existing chemotaxis computational modeling to include non-canonical messengers. Non-canonical signals being involved in the chemotaxis pathway appears to be more prevalent in environmental bacteria than in domesticated chemotaxis model strains. Chemotaxis genes are also often essential for virulence in potentially pathogenic bacteria species. Many bacterial systems of study involve motility and chemotaxis, but this aspect is often understudied. The computational models presented here provide an additional tool to efficiently investigate the role of chemotaxis in non-model bacterial systems.

CHAPTER 3: MICROFLUIDIC DEVICES TO CREATE COMPLEX ENVIRONMENTS

Introduction

It has been observed that bacterial rhizosphere communities are enriched for chemotaxis genes compared to bulk soil[4]. When examined directly, plant growth promoting bacteria that are chemotactic appear to be using chemotaxis to navigate to the surface of roots[5]. This is all suggestive that chemotaxis is an important part of root colonization and rhizosphere community assembly.

However, there are outstanding complicating aspects of this system. First, soil bacteria have more chemotaxis and motility genes than the domesticated chemotaxis model *Escherichia coli*[10]. Second, the physical and chemical structure of soil is complex temporally and spatially[2,6]. Pore spaces are narrow and convoluted, creating a maze between bacteria in the bulk soil and the surface of a root[2,6]. Chemically soil includes many overlapping signals, including but not limited to pH, oxygen, root exudates, and decomposition products[2,6]. It is not clear how soil bacteria transduce all the chemical signals and navigate through the maze of soil pores to the surface of a root. We know that soil bacteria tend to have multiple copies of each chemotaxis gene in the pathway, a significantly larger diversity of chemoreceptors, and domains in some of their chemotaxis enzymes that suggest the incorporation of non-canonical internal signals in addition to canonical functions[10].

As a model organism to explore the means of navigating the complex soil systems, we are looking at *Azospirillum brasilense*. *A. brasilense* is a plant growth promoting bacterium isolated from the roots of cereal crops[11]. It has a chemotaxis pathway that is representative of rhizosphere bacteria chemotaxis machinery[55]. Specifically, it has around 50 annotated chemoreceptors, 4 chemotaxis operons, several copies of chemotaxis enzymes like CheA, CheW, and CheY, and several of the chemoreceptors have c-di-GMP binding domains[5,20,26,55]. Additionally, it is the most abundant bacterial additive in green fertilizers[1], so there are commercial implications in understanding *A. brasilense*'s chemotaxis pathway specifically as well as the expectation of gaining insight into soil bacteria generally. Under laboratory conditions, *A. brasilense* performs precision chemotaxis, forming bands at optimal concentrations based on the redox state of the cell compared to the redox potential of the gradient[12]. The binding of c-di-GMP to chemoreceptors has been shown to alter the band formation phenotype of *A. brasilense in vitro*[5,20,26]. However, c-di-GMP is not involved in canonical chemotaxis signaling and it is not clear how it alters signal transduction to achieve the observed phenotype. As the mechanism of

c-di-GMP signal transduction is not understood, appears to be important for precision energy taxis in *A. brasilense*, and would shed light on other instances of non-canonical signal transduction, we sought to investigate how shifting c-di-GMP activity changes precision taxis in varying chemical and physical landscapes.

To investigate the role of c-di-GMP in *A. brasilense* precision energy taxis, we planned to test conditions that would discriminate between models of interaction based on computational modeling results. That required us to have control over both the environment and the biochemistry of the cells. The level of environmental control that we expected to be necessary is not afforded by the current standard capillary assay used to investigate *A. brasilense* chemotaxis[12]. The capillary assay is effective for creating an oxygen gradient but does not control for other potential gradients in the system and requires a high density of cells[12]. These conditions may lead to the creation of an opposed carbon gradient generated by leftover carbon intended to keep the cells motile when preparing them for the assay, or secondary attractant gradients created by cells that sense an attractant and release a second strong attractant to increase the number of sister cells migrating towards a potential food source. To control for these factors, we decided to work with microfluidic systems where we would have greater control over the chemical and physical environment. With a microfluidic system we could, in theory, generate arbitrarily shaped chemical landscapes with physical obstacles of our design, meaning that we could test overlapping gradients, non-linear gradients, and physical convolution that more closely replicated soil pore spaces.

In addition to environmental control, we also needed some amount of control over the internal biochemistry of the *A. brasilense*, specifically the activity of c-di-GMP. Past work done by our collaborators in the Alexandre lab already generated relevant mutant strains for this purpose[5,18,20,31,56]. On the receptor side, mutants knocking out receptors with c-di-GMP binding domains or knocking out just the c-di-GMP binding domains in those receptors have been made and investigated using the capillary assay[5,20]. Strains that use specific wavelengths of light to signal activity, also known as optogenetic strains[57], were made for a diguanylate cyclase (DGC) that produces c-di-GMP and a phosphodiesterase (PDE) that depletes c-di-GMP[26]. We planned to use these strains in microfluidic systems to test how changing the activity of c-di-GMP, either by changing the amount of c-di-GMP in the cell or by using cells with altered sensitivity to c-di-GMP, changed chemotaxis behavior.

Microfluidics is a commonly used technology to study chemotaxis as it provides a high level of control over the physical and chemical environment on a scale that is relevant for bacteria[38–41]. Microfluidics most commonly uses devices made of poly-dimethylsilane (PDMS), an optically

clear rubber that is permeable to non-polar compounds and gases while impermeable to hydrophilic solutes or polar liquids like water[58]. In past work exploring chemotaxis with hydrophilic attractants, gradients have been formed by having two large reservoirs with different concentrations of attractant and examining chemotaxis in a bridge region directly connecting the two reservoirs[46], by using microslits to connect a flow channel to an observation chamber[52], or by using a hydrogel to make the device instead of PDMS[48,51,59–61]. All of these options result in stable linear gradients but struggle to form stable non-linear gradients. Exponential gradients are naturally relevant due to the logarithmic sensitivity of bacterial cells to attractants[7] and because environmental gradients appear near-exponential before either stabilizing or dissipating[62]. Unfortunately, past microfluidic design principles were inadequate to meet our needs.

To design a device that would generate and support a non-linear chemoattractant gradient, we started with diffusion modeling to develop a design. The modeling suggested that creating non-linear gradients requires that edges of a region be held at constant concentration. While PDMS is the most common material for microfluidic devices[58], work has been done in a wide variety of different materials, ranging from paper to rock to glass[42,63–65], but of the greatest interest is hydrogels[61]. Hydrogels such as agarose or polyethylene glycol (PEG) allow for the diffusion of small hydrophilic chemoattractants but they are more fragile than PDMS and prone to drying out and breaking in the air. A method for grafting PEG onto PDMS has been developed[53], and we decided to adapt this method to maintain the structural advantages of PDMS while incorporating the desired permeability of PEG in select regions. We applied this technological approach to our design and created devices that were able to generate and sustain overlapping exponential gradients. In so doing, we have developed a design method that gives us the level of environmental control that we need to test the predictions from our computational modeling of *A. brasilense* chemotaxis behavior. It is expected that being able to generate overlapping exponential gradients would be necessary to discriminate between potential models of c-di-GMP signal transduction. However, we were not able to put cells into the system at time of writing due to fragility of the devices.

Materials & Methods

Media and strains

Strains of *A. brasilense* were provided by the Alexandre lab from their previously published work (table 3.1). These include optogenetic strains (strains with a specific activity linked to exposure to specific wavelengths of light) for DGC and PDE activities. Media and growth conditions for *A. brasilense* match published work, with the addition of polyvinylpyrrolidone (PVP) to passivate

the system as published in other work. *E. coli* MG1655 was also used to validate the system and was grown according to previous publications.

When making gradient systems, chemotaxis media appropriate for the microbe was used, M9-Chemotaxis for *E. coli* MG1655 and CBAB for *A. brasilense* strains. The attractant used for *E. coli* was L-Serine or tryptone as *E. coli* is most sensitive to serine and aspartate as chemoattractants. For *A. brasilense* malate was used following published protocols. To track the gradients, fluorescent dyes were added with the attractants. These have been shown to have similar diffusion properties to the small polar organic molecules used as attractants. In general, two dyes were used: fluorescein and Rhodamine B.

To match the capillary assay, work an oxygen gradient was attempted. For this sodium sulfite was added to scavenge oxygen and tris(bipyrinidine)ruthenium(II) chloride ($Ru(BPY)_3$) was used as a fluorescent indicator of oxygen concentration in the system.

For all the microscopy work, 0.1% PVP was added to the media to passivate the system following published protocols.

Table 3.1. Summary of described deletion strains. Deletion strains developed by the Alexandre lab at time of writing, the chemotaxis phenotypes in the band formation capillary assay, and where the strain is described in the literature.

Strain	Band phenotype compared to Sp7	Citation
Δaer	Further from meniscus	[5]
Δaer (AerΔPilZ)	Diffuse (+N), closer (-N)	[5]
ΔcheY1	Slower formation	[31]
ΔcheY4	No band	[31]
ΔcheA4	No band	[31]
Δche4	No band	[31]
Δtlp1	Further from meniscus (2 min), closer to meniscus (5 min), dissipates early (at or before 15 min)	[20]
Δtlp1 (Tlp1ΔPilZ)	Phenocopies Δtlp1	[20]
ΔcheA1	No change	[56]
ΔcheY1	Further from meniscus	[56]
Δche1	Further from meniscus	[56]
ΔcheB1ΔcheR1	Further from meniscus	[18]

Microscopy

For the present work, a Nikon Eclipse Ti microscope was used. All movies used the 10x objective. For fluorescent tracking of beads, Rhodamine B, and fluorescein, premade DAPI, RFP and GFP blocks were used respectively.

Computational analysis

To analyze the microscopy data, taking movies of cells swimming and turning them into tracks and then analyzing those tracks to pull out metrics about the swimming of the cells, custom MATLAB scripts were used as in previous publications.

Capillary assay

Capillary assay was done as previously published to ensure standard chemotactic behavior between labs. In brief, *A. brasilense* cells were cultured in minimal media containing malate as a carbon source into exponential growth. The cells were then washed into the CBAB with fructose and concentrated to ~10^8 cells/mL. This cell suspension is then draw into a glass capillary by capillary action and allowed to form a natural oxygen gradient by aerobic respiration depleting the dissolved oxygen. Cells are observed forming a band near the meniscus.

Microfluidics

To briefly overview the method we used to produce custom microfluidic devices: a custom mask is drawn using computer assisted drawing software and printed; the mask is used to generate a mold in polymethyl-methacrylate (PMMA) on a clean silicon wafer and the mold is silanized to make it non-reactive; an optically clear rubber, polydimethyl-silane (PDMS), is poured over the mold and cured, then cut out; cut PDMS shells and glass cover slips are exposed to oxygen plasma, assembled, and heated to form a covalently bound shell to fill with liquid.

For “hybrid” devices, the shells were cut off the molds and port holes were punched in the shells. Then the shells were soaked in a benzophenone solution (10% m/v in acetone, 1 min), rinsed (10 s each with MeOH and dd H_2O), exposed to oxygen plasma (1 min), and assembled with a glass cover slip. This process created a device with a benzophenone doped shell. The assembly was not exposed to heat as this degraded the benzophenone. The device was filled with a PEG-DA solution (40% v/v in dd H_2O) and the device was selectively exposed to UV using a mask. The UV causes the PEG-DA to polymerize, and the benzophenone reacts with the PEG-DA and PDMS shell as a linker, allowing the PEG walls formed to be anchored into the PDMS shell covalently. The hybrid devices were then attached to flow systems that flowed media, media containing attractant and dye, or media containing motile cells around the outside of the central chamber. The flow in this system was entirely gravity based, no positive pressure was applied to the system.

Custom microfluidic designs were used (figure 3.1, 3.2). CAD software was used to draw designs that were then printed as masks. Designs used hexagonal tessellation of support pillars to minimize the number of supports required and round curves in flow channels to minimize eddies in flow channels. A version of the 2 square chamber device was produced to replicate

the simple gradients published in Colin R, et al (2014) (figure 3.1A). The 2-chamber device is a simple baseline for looking into chemotaxis in a single linear gradient, and we used it to validate that strains were capable of chemotaxis in a published design. To create a gas gradient, a replica of the design published by Morse M, et al (2016), was made and used (figure 3.1B). The 3-channel device also produces a linear gradient, but in a gas, so when placed in a controlled atmosphere chamber it is an appropriate device to examine chemotaxis in an oxygen gradient (aerotaxis).

In addition to being effective at analyzing motility and chemotaxis, microfluidics is also widely used to investigate growth with high definition for individual cell phenotype. In general, these devices are based on principles laid out for micro-chemostats, or “mother machines”, developed by Wang et al (2010)[66]. We sought to extend that design by adding mixing to the process[67–71] to generate a mother machine that contains a pseudo non-linear gradient made up of two linear gradients of different slopes (figure 3.1C). Our resulting “mother tree” design ended up not being necessary for any of the projects in our lab but was intended to be used with an inducer gradient to examine with high resolution the growth costs of induced expression of genetic constructs, like inducible flagellar expression for example, and thus parse the actual tradeoff between growth and expression of individual genes.

For the hybrid microfluidic devices, two masks were made, one for the PDMS shell and one for the PEG walls to be produced within. The design for the hybrid device is a central chamber with PEG walls that describe a hexagon creating six flow channels around the outside of the central chamber. One of the PEG walls has a gap to allow for cells to enter from the flow channel on that side. We took this principle in two directions: a simple central chamber surrounded by flow channels (figure 3.2A), and a long rectangular channel with flow channels on the sides (figure 3.2B). While both designs can create overlapping and non-linear gradients, the central chamber “snowflake” design is more focused on creating overlapping gradients, so it’s a better device to use for testing how sensation of overlapping gradients combine to produce chemotaxis behavior. The longer channel offers more control over the shape of the gradient, but less control over the angles, so this device is better for testing how cells adapt to gradients (e.g., logarithmic sensation or linear sensation).

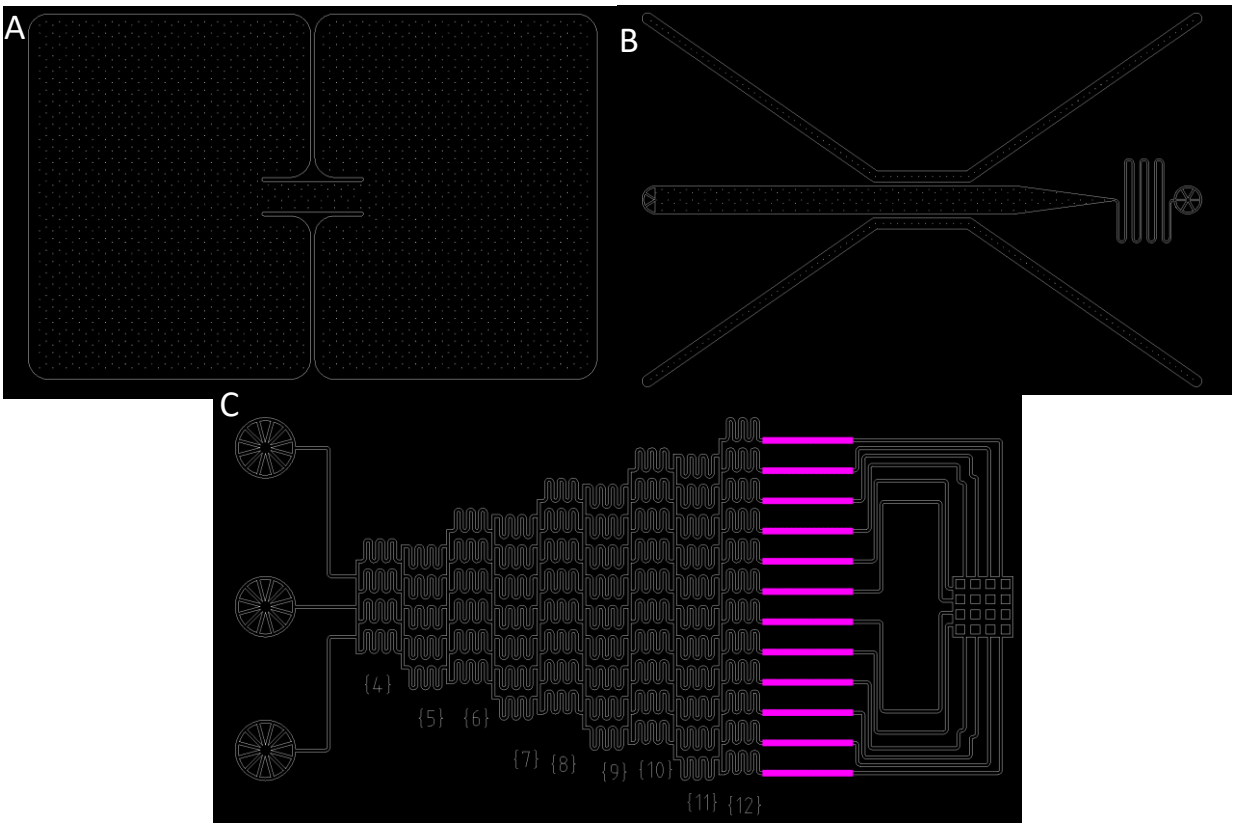

Figure 3.1. Designs for microfluidic devices using PDMS. (A) 2-chamber device where each chamber is filled with a solution of cells, one side has attractant and the other does not. A linear gradient forms in the bridge and is tracked with a fluorescent dye such as fluorescein. Design adapted from Colin, R., et al (2014)[46]. (B) 3-channel device where the side channels have constant flow, and the central channel contains cells. One side channel contains a gas solvated solution while the other two channels contain solutions without any of the gas. A linear gas gradient forms in the center channel perpendicular to the flow direction and can be tracked with a gas sensitive fluorophore, such as $Ru(BPY)_3$ in the case of an oxygen gradient. Design adapted from Morse, M., et al (2016)[47]. (C) Mother tree device that will produce a gradient of inputs for a micro-chemostat system. Media flows in from the wagon wheels on the left side and go through several rounds of mixing before reaching the cross channels (magenta) where the cells grow, then go out via a single outlet. The single outlet ensures pressure is equalized through the system and simplifies the piping needed to set things up. Growth channel widths are on the order of the width of a cell.

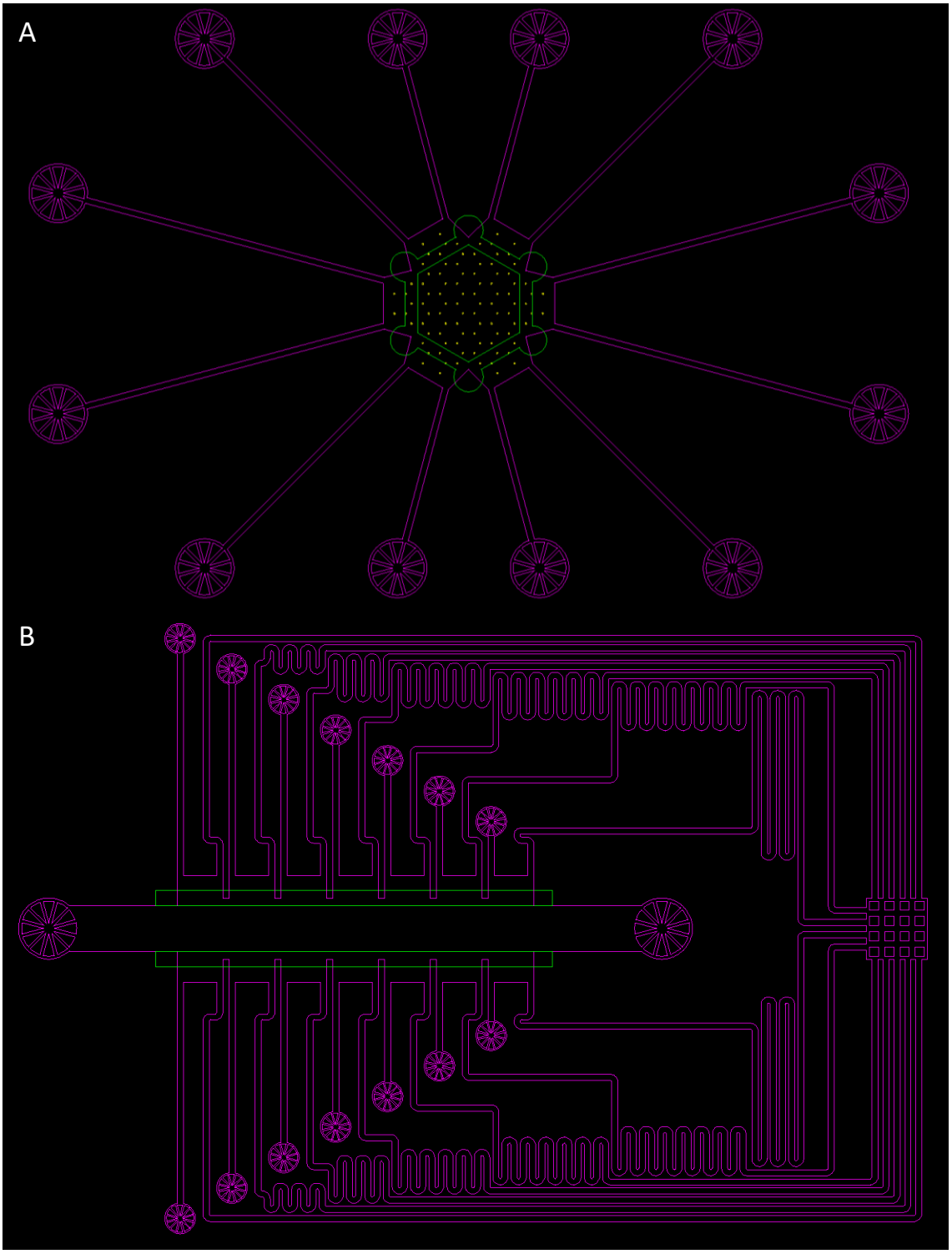

Figure 3.2. Designs for microfluidic devices that use hybrid materials (both PDMS and PEG). PDMS walls are shown in magenta, support pillars are also produced in PDMS and are shown in yellow, the PEG walls are shown in green. (A) The central chamber “snowflake” device consists of a central hexagonal chamber with channels that flow across the sides. The walls

Figure 3.2 (cont'd)
separating the central chamber from the flow channels are made of PEG, allowing for the diffusion of hydrophilic solutes. By varying the concentration of solutes in each flow channel we can control the chemical landscape in the central chamber. (B) The long channel "Manhattan" device consists of a large central channel that contains cells and several short flow channels that go across the sides. The walls separating the flow channels from the central channel are made of PEG, so varying the solute concentration in each flow channel allows us to control the chemical landscape in the central channel.

Diffusion modeling

To design a microfluidic device that would create a non-linear gradient, diffusion modeling was used to generate an initial concept. For computational efficiency, thermal diffusion equations were used because they resolve more quickly than liquid diffusion models and are the same if we ignore turbulent flows. MATLAB has built in functions defining thermal diffusion in a user defined shape that were used.

Results

Capillary band formation

As proof of principle, the WT strain *A. brasilense* Sp7 and the two optogenetic strains, one for DGC activity and one for PDE activity, were assayed for band formation using the published capillary assay. Band formation behavior was shown to change in the optogenetic strains when exposed to inducing wavelengths of light, showing that we were able to replicate previously published results using the capillary assay (figure 3.3).

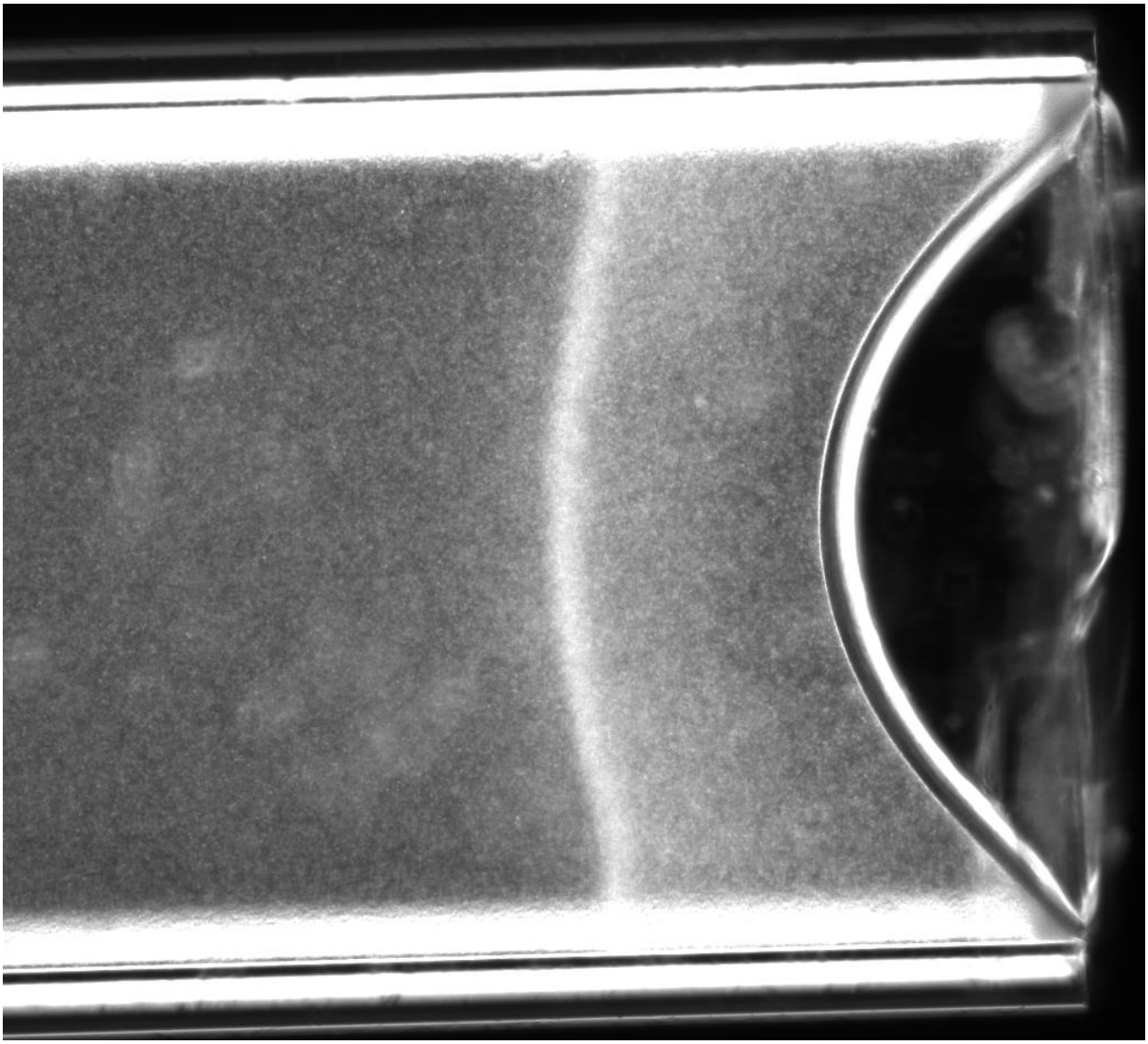

Figure 3.3. Band formation of Azospirillum brasilense in a glass capillary tube at an optimal concentration of dissolved oxygen. Cells are grown in minimal media supplemented with labile nitrogen, then washed into chemotaxis media and concentrated to ~10^9 cells/mL and loaded into a glass capillary tube via capillary action. At that high cell density, they rapidly consume oxygen and naturally create an oxygen gradient in the capillary tube. We image the cells on the microscope after ~5 mins using bright field lighting and 4x magnification (40x total magnification). The image above is a representative band of the wildtype A. brasilense (Sp7). The band forms at 0.4% dissolved oxygen. Cells at higher oxygen concentrations clump and begin to form cysts while cells at lower oxygen concentrations simply stop moving.

Chemotaxis in basic microfluidic gradients

To understand how cells respond to environmentally relevant gradients, it is necessary to develop a microfluidic system that allows for the creation of non-linear and overlapping gradients. As a baseline, we tested cells' chemotaxis in simple linear gradient systems. We showed that we were able to establish a stable gradient with which to do the work and measured the chemotaxis of *E. coli* MG1655 and *A. brasilense* Sp7 in simple gradient systems.

Creating an oxygen gradient device

The gradient that is formed in the capillary assay is primarily an oxygen gradient and the band forms at 0.4% O_2. To match those data most closely we worked to design and create a microfluidic device that established an oxygen gradient. PDMS allows for the diffusion of non-polar gases such as oxygen and previous work has shown that gas gradients can be made, so it should be a simple matter of replicating the existing design. The limitation that we ran into was that we don't have an anaerobic chamber to do microscopy in, and acquiring one was beyond the financial scope of the project. In the literature it is also shown that chemicals can be added to scavenge oxygen in liquid systems, most easily sodium sulfite. There is also a readily available oxygen sensitive fluorescent dye called $Ru(BPY)_3$. Unfortunately, our abiotic trials showed that while sodium sulfite did scavenge oxygen, it did not reduce the dissolved oxygen to 0.4%, which is the concentration where the band forms for the wildtype strain.

Diffusion modeling to design non-linear gradient devices

We used diffusion modeling to inform the way we designed a device to produce a non-linear gradient. To save on computational time we used thermal diffusion models built into MATLAB to get a qualitative sense of how to produce an exponential gradient. We found that when all of the edges of a shape are help at a constant concentration or temperature it is possible to create gradients of arbitrary shape. For example, if all but one side are held at the same concentration or temperature and the odd side out is held at a higher concentration or temperature, then the gradient radiating out from that side will be exponential (figure 3.4).

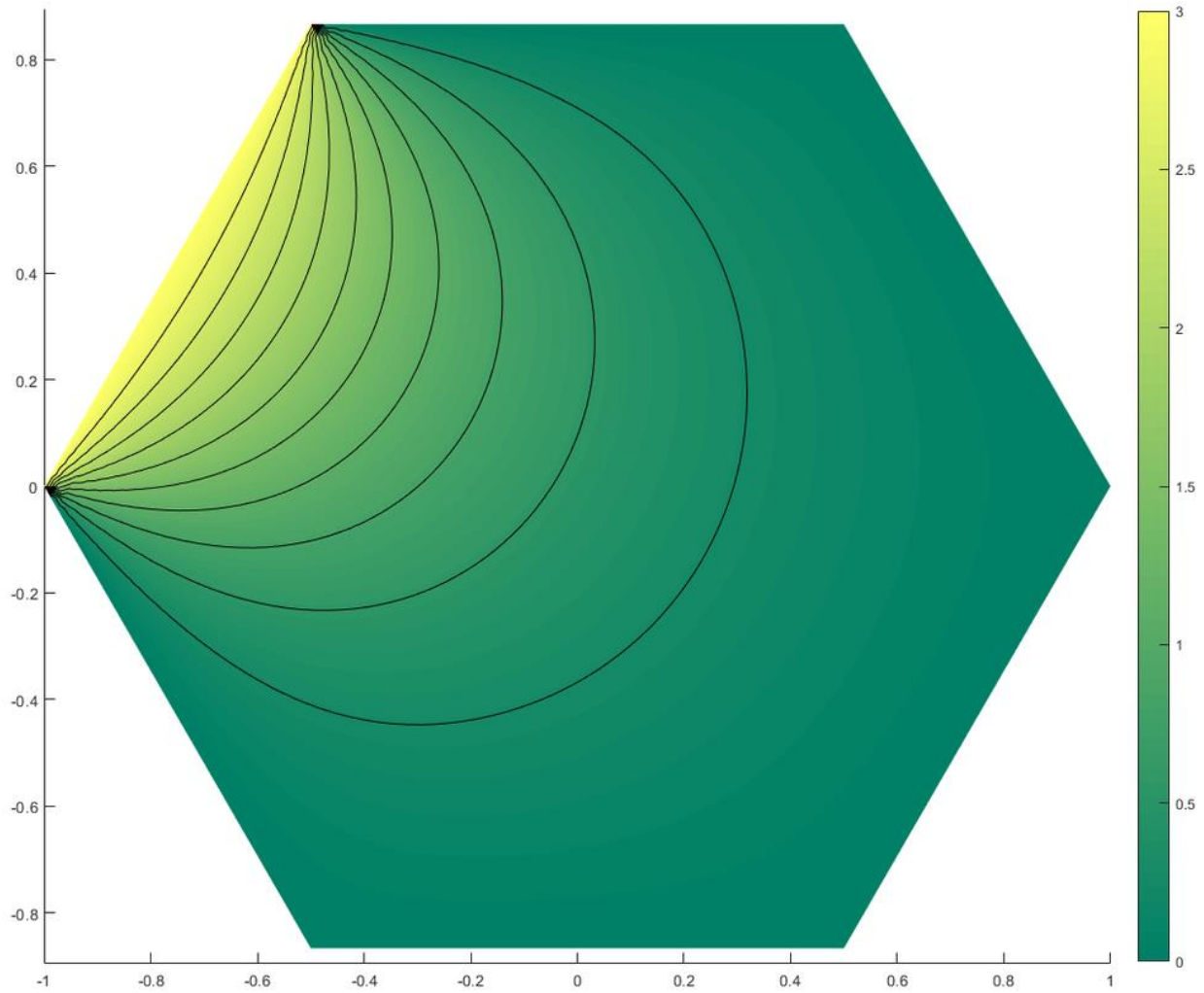

Figure 3.4. Thermal conductivity modeling predicts that it is possible to form exponential gradients in closed chambers. Thermal conductivity models are qualitatively the same as solute diffusion models and computationally less taxing. By holding all but one of the edges at a constant low concentration while the last edge is held at a high concentration, an exponential gradient should form.

Hybrid microfluidic devices create non-linear gradients

The diffusion models predicted that holding the edges of a chamber at constant concentrations would yield stable non-linear gradients. To do that, we need a way to create walls that are permeable to the solutes of interest and a way to hold the concentrations on the outsides of the walls constant. The first issue is solved by grafting a hydrogel into the PDMS shell. This combination of materials grants more control over the shape of the gradients than if we used only PDMS or only hydrogel. The latter issue could be addressed either through having large reservoirs outside the main chamber or by flowing media across the walls in a flow system. We

decided that the latter would be more effective and the technique more broadly applicable to other potential future systems of interest. Troubleshooting the technique to graft the hydrogel into the PDMS led us to settling on a simpler combination of chemicals and older technique. The main issue was having the polymerize too quickly and failing to graft into the PDMS. Later it became clear that the connection between the hydrogel and the glass cover slip was weak and broke easily, so fluorescent beads were added to the media to track flow directly. This additionally provided a means of measuring the diffusion on non-motile particles in the system. We successfully made hybrid devices that have stable exponential gradients (figure 3.5). However, troubleshooting the addition of chemotactic cells to the system is incomplete. At present, there is an outstanding issue of fragility in the system. Specifically, any jostling or addition of positive pressure to the system causes the hydrogel-glass junction to separate irreparably.

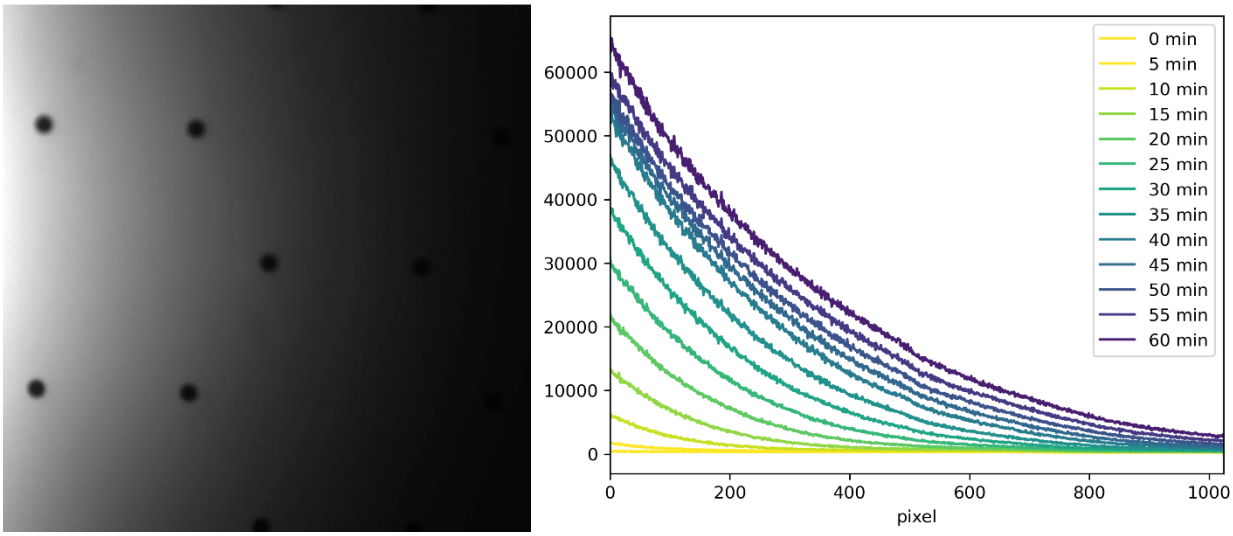

Figure 3.5. Over time an exponential gradient of fluorescent dye forms in a hybrid PEG-PDMS microfluidic device. A fluorescein solution was flowed past a hydrogel wall on one side of a central chamber while buffer was flowed past each of the other walls. Fluorescent images were collected in the central chamber at regular intervals. (Left) A sample fluorescent image of the chamber near the source wall after 30 min shows qualitative similarity to the thermal conductivity model. (Right) Gradient intensity vs distance from the source plotted for images taken 5 min apart. Fluorescence is directly related to the concentration of the dye under tested conditions and shows a clear establishment of an exponential gradient within 10 min. The gradient continues to approach its equilibrium, but on the time scale of our experiments the gradient is stable.

Discussion

Novel microfluidics

Ideas for using hydrogel walls, grafting those walls into a PDMS shell, and non-linear gradient formation have all been worked on before, but the combination of those ideas into a microfluidic design method is novel. Starting with diffusion modeling, we surmised that holding the edges of a central chamber at constant concentrations would result in gradients of arbitrary shape. We manufactured one of our designs grafting PEG onto PDMS. The resulting device had a central chamber surrounded by PEG walls that separated the chamber from the flow channels. We demonstrated that this design allowed for the generation of exponential gradients that can overlap at arbitrary angles. As natural gradients start as pseudo-exponential, having access to a device that can create exponential gradients is relevant to microbial research broadly.

Known issues and future directions

The biggest issue with the designs that were tested is their fragility. As PEG-DA is toxic to cells it may act as a chemorepellent or otherwise interfere with chemotaxis assays. This means it is necessary to rinse out the device with media as part of setting it up. However, the fragility of the system complicates this, specifically the weak interaction between the glass and the PEG walls. While there is a concern that without heating the PDMS-glass device there won't be proper adhesion between the PDMS and glass, in our experience this isn't an issue so long as both the PDMS and glass are well cleaned prior to plasma treatment and assembly. The PEG-glass interface however has no covalent bond, so to prevent flow under the PEG walls we are relying on van der Waals interactions and stearic occlusion. Neither are strong, so if any positive pressure is introduced into the system at all, the PEG-glass interface comes apart to relieve the pressure.

Managing the fragility of the PEG-glass interface is likely manageable through careful manipulation and set up of the device, but for a more reliable answer some amount of redesign would be more robust. The first suggestion is to use the microscope's built-in UV lamp to do the exposure instead of masking. If the issue is due to incomplete polymerization of the walls, using the microscope's UV lamp and computerized stage control may be effective. However, the width of the walls must be wider as there is significant propagation of the radical polymerization reaction and the process is overall slower than masking so the risk of drying the device out during set up is higher. Another method would be replacing the glass cover slip with a PDMS slab. Creating a uniformly thin and relatively rigid PDMS slab is a more difficult technique than using glass, and a PDMS slab is likely necessarily going to be thicker than the cover slip.

However, this has the advantage of allowing the PEG to graft onto both the top and bottom of the device and thereby reducing fragility.

CHAPTER 4: CONCLUSIONS

As climate change and population increases pressure global agriculture, creative and climate neutral solutions are being sought. One such solution is “green fertilizers”, mixtures of microbes known to associate with plant roots and provide both resistance to stresses and improve crop yield. A bacterium common in green fertilizers is *A. brasilense*. *A. brasilense* is known to use its chemotaxis machinery to navigate to the roots of plants *in vitro*, and while its chemotaxis pathway is like that of *E. coli*, several of its chemoreceptors have internal binding domains for c-di-GMP as well as ligand binding domains. When internal levels of c-di-GMP change, *A. brasilense* has been shown to alter its chemotaxis behavior. This leaves open the question of how c-di-GMP binding is altering chemotactic signal transduction to result in the altered behavior.

To investigate this system, we determined that a combination of computational modeling and custom microfluidics would be the most efficient and direct methodology. Computational modeling provides a way to examine the logical and causal interactions that result in the chemotaxis phenotype, and it is a resource efficient and relatively fast means to narrow the number of potential hypotheses that are consistent with past observations. Computational modeling also predicts new conditions that discriminate between hypotheses. To test those new conditions, it is helpful to leverage the environmental control at bacterially relevant scale provided by microfluidics. Each of these methods required developing new tools.

Agent based computational models for *E. coli* were adapted for *A. brasilense*. Existing models were adapted from MATLAB to Python 3.8, making them more accessible for future research and adaptation to other systems. In addition, 3-dimensionality was added to the system as well as a computationally efficient way of calculating random changes in orientation in 3-D using quaternions[72], a technique widely used in other 3-D systems. We also adapted the math from other work showing that tumble angle can be accurately modeled in the same way that Brownian shifts to angle during runs are modeled[37], which also streamlines the computation.

The computational models and hybrid microfluidics designs are broadly applicable to other systems. Microfluidic designs have historically struggled to produce stable exponential and other non-linear gradients, and in this work we created designs that produce stable exponential gradients. By applying diffusion modeling we settled on the foundational concept that holding the sides of a central chamber at constant concentrations would create an exponential gradient. From there we combined concepts from hydrogel devices with techniques for grafting the hydrogel PEG onto a PDMS shell[53]. By doing this we were able to create an exponential gradient as a proof of concept (figure 3.5).

Motility and chemotaxis are commonly associated with pathogenesis[73] and these aspects of pathogenesis are not as thoroughly or commonly studied as other pathogenesis markers. Additionally, pathogenic bacteria often need to navigate hydrogel/mucosal systems to establish an infection, such as in the GI track or the airways[73]. This work demonstrates that existing tools can be adapted to specific environments, that is we have laid the technical groundwork for application to a wider range of other model systems. The work here was aimed at understanding the signaling pathway underlying the colonization of roots in a soil system, and the same tools could be used to answer questions more directly aimed at the colonization process (e.g., in a fake soil, does varying the amount of total CheY determine ability to respond to a root exudate chemoattractant and reach a fake root?), or to extend research on the role of pH in pathogen motility in hydrogels similar to intestinal mucus to the role of pH in pathogen chemotaxis in mucus-like hydrogels.

On the basic side, short-lived small molecule messengers appear to be biologically ubiquitous and due to their short lifespans, they remain difficult to study directly[29]. The present work provides a path for researching how these interactions may result in observable downstream behavior with computational modeling, and a means to refine those models using microfluidic devices.

Overall, the work presented in here lays out the technical means to answer the question that was initially proposed. These same methods and technologies can be broadly applied to other questions and demonstrate the power of computational modeling and microfluidics to aid in biological research, both on their own and in conjunction.

REFERENCES

1. Ryan, P. R., Dessaux, Y., Thomashow, L. S. & Weller, D. M. Rhizosphere engineering and management for sustainable agriculture. *Plant and Soil* vol. 321 363–383 Preprint at https://doi.org/10.1007/s11104-009-0001-6 (2009).
2. Lareen, A., Burton, F. & Schäfer, P. Plant root-microbe communication in shaping root microbiomes. *Plant Molecular Biology* vol. 90 575–587 Preprint at https://doi.org/10.1007/s11103-015-0417-8 (2016).
3. Meena, V. S. *et al.* Plant beneficial rhizospheric microorganism (PBRM) strategies to improve nutrients use efficiency: A review. *Ecol Eng* **107**, 8–32 (2017).
4. Buchan, A., Crombie, B. & Alexandre, G. M. Temporal dynamics and genetic diversity of chemotactic-competent microbial populations in the rhizosphere. *Environ Microbiol* **12**, 3171–3184 (2010).
5. O'Neal, L., Akhter, S. & Alexandre, G. A PilZ-Containing Chemotaxis Receptor Mediates Oxygen and Wheat Root Sensing in Azospirillum brasilense. *Front Microbiol* **10**, 1–10 (2019).
6. Hinsinger, P., Gobran, G. R., Gregory, P. J. & Wenzel, W. W. Rhizosphere geometry and heterogeneity arising from root-mediated physical and chemical processes. *New Phytologist* vol. 168 293–303 Preprint at https://doi.org/10.1111/j.1469-8137.2005.01512.x (2005).
7. Karmakar, R. State of the art of bacterial chemotaxis. *Journal of Basic Microbiology* vol. 61 366–379 Preprint at https://doi.org/10.1002/jobm.202000661 (2021).
8. Colin, R., Ni, B., Laganenka, L. & Sourjik, V. Multiple functions of flagellar motility and chemotaxis in bacterial physiology. *FEMS Microbiology Reviews* vol. 45 Preprint at https://doi.org/10.1093/femsre/fuab038 (2021).
9. Berg, H. C. & Brown, D. A. *Chemotaxis in Escherichia coli analysed by Three-dimensional Tracking*. *NATURE* vol. 239 (1972).
10. Mukherjee, T. *et al.* Multiple CheY Homologs Control Swimming Reversals and Transient Pauses in Azospirillum brasilense. *Biophys J* **116**, 1527–1537 (2019).
11. Okon, Y. & Labandera-Gonzalez, C. A. AGRONOMIC APPLICATIONS OF AZOSPIRILLUM: AN EVALUATION OF 20 YEARS WORLDWIDE FIELD INOCULATION. *Soil Biology Biochemistry* **26**, 1591–1601 (1994).
12. O'Neal, L., Mukherjee, T. & Alexandre, G. Analyzing Chemotaxis and Related Behaviors of Azospirillum Brasilense. in *Current Protocols in Microbiology* 3E.3.1-3E.3.11 (John Wiley & Sons, Inc., 2018). doi:10.1002/cpmc.49.
13. Li, H., Cui, Y., Wu, L., Tu, R. & Chen, S. cDNA-AFLP analysis of differential gene expression related to cell chemotactic and encystment of Azospirillum brasilense. *Microbiol Res* **166**, 595–605 (2011).
14. Wu, L., Cui, Y., Hong, Y. & Chen, S. A CheR/CheB fusion protein is involved in cyst cell development and chemotaxis in Azospirillum brasilense Sp7. *Microbiol Res* **166**, 606–617 (2011).
15. Kadouri, D., Jurkevitch, E. & Okon, Y. Involvement of the reserve material poly-β-hydroxybutyrate in Azospirillum brasilense stress endurance and root colonization. *Appl Environ Microbiol* **69**, 3244–3250 (2003).

16. Mukherjee, T., Kumar, D., Burriss, N., Xie, Z. & Alexandre, G. *Azospirillum brasilense chemotaxis depends on two signaling pathways regulating distinct motility parameters*. *Journal of Bacteriology* vol. 198 (2016).

17. O'Neal, L. *et al.* Distinct Chemotaxis Protein Paralogs Assemble into Chemoreceptor Signaling Arrays To Coordinate Signaling Output. *mBio* **10**, 1–16 (2019).

18. Stephens, B. B., Loar, S. N. & Alexandre, G. Role of CheB and CheR in the complex chemotactic and aerotactic pathway of Azospirillum brasilense. *J Bacteriol* **188**, 4759–4768 (2006).

19. Carreño-López, R., Sánchez, A., Camargo, N., Elmerich, C. & Baca, B. E. Characterization of chsA, a new gene controlling the chemotactic response in Azospirillum brasilense Sp7. *Arch Microbiol* **191**, 501–507 (2009).

20. Russell, M. H. *et al.* Integration of the second messenger c-di-GMP into the chemotactic signaling pathway. *mBio* **4**, 1–11 (2013).

21. Zhulin, I. B., Bespalov, V. A. & Taylor, B. L. Oxygen Taxis and Proton Motive Force in Azospirillum brasilense. *Microbiology (N Y)* **178**, 5199–5204 (1996).

22. Mazzag, B. C., Zhulin, B. & Mogilner, A. Model of Bacterial Band Formation in Aerotaxis. *Biophys J* **85**, 3558–3574 (2003).

23. Alexandre, G., Greer, S. E. & Zhulin, I. B. Energy Taxis Is the Dominant Behavior in Azospirillum brasilense. *Society* **182**, 6042–6048 (2000).

24. Alexandre, G., Greer-Phillips, S. & Zhulin, I. B. Ecological role of energy taxis in microorganisms. *FEMS Microbiol Rev* **28**, 113–126 (2004).

25. Greer-Phillips, S. E., Stephens, B. B. & Alexandre, G. An energy taxis transducer promotes root colonization by Azospirillum brasilense. *J Bacteriol* **186**, 6595–6604 (2004).

26. O'Neal, L., Ryu, M., Gomelsky, M. & Alexandre, G. Optogenetic Manipulation of Cyclic Receptor Activity in Azospirillum. *J Bacteriol* **199**, 1–18 (2017).

27. Sourjik Rü diger Schmitt, V. *Different roles of CheY1 and CheY2 in the chemotaxis of Rhizobium meliloti*.

28. Lertsethtakarn, P., Howitt, M. R., Castellon, J., Amieva, M. R. & Ottemann, K. M. Helicobacter pyloriCheZHP and ChePep form a novel chemotaxis-regulatory complex distinct from the core chemotaxis signaling proteins and the flagellar motor. *Mol Microbiol* **97**, 1063–1078 (2015).

29. Petchiappan, A., Sujay, &, Naik, Y. & Chatterji, D. Tracking the homeostasis of second messenger cyclic-di-GMP in bacteria. doi:10.1007/s12551-020-00636-1/Published.

30. Ryjenkov, D. A., Simm, R., Römling, U. & Gomelsky, M. The PilZ domain is a receptor for the second messenger c-di-GMP: The PilZ domain protein YcgR controls motility in enterobacteria. *Journal of Biological Chemistry* **281**, 30310–30314 (2006).

31. Mukherjee, T., Kumar, D., Burriss, N., Xie, Z. & Alexandre, G. Azospirillum brasilense chemotaxis depends on two signaling pathways regulating distinct motility parameters. *J Bacteriol* **198**, 1764–1772 (2016).

32. Waite, A. J. *et al.* Non-genetic diversity modulates population performance. *Mol Syst Biol* **12**, 895 (2016).

33. Frankel, N. W. *et al.* Adaptability of non-genetic diversity in bacterial chemotaxis. *Elife* **3**, 1–30 (2014).

34. Dufour, Y. S., Fu, X., Hernandez-Nunez, L. & Emonet, T. Limits of Feedback Control in Bacterial Chemotaxis. *PLoS Comput Biol* **10**, e1003694 (2014).

35. Dufour, Y. S., Gillet, S., Frankel, N. W., Weibel, D. B. & Emonet, T. Direct Correlation between Motile Behavior and Protein Abundance in Single Cells. *PLoS Comput Biol* **12**, 1–25 (2016).

36. Hu, B. & Tu, Y. Behaviors and Strategies of Bacterial Navigation in Chemical and Nonchemical Gradients. *PLoS Comput Biol* **10**, (2014).

37. Saragosti, J., Silberzan, P. & Buguin, A. Modeling E. coli tumbles by rotational diffusion. implications for chemotaxis. *PLoS One* **7**, e35412 (2012).

38. Rusconi, R., Garren, M. & Stocker, R. Microfluidics Expanding the Frontiers of Microbial Ecology. *Annu Rev Biophys* **43**, 65–91 (2014).

39. Hol, F. J. H. & Dekker, C. Zooming in to see the bigger picture: Microfluidic and nanofabrication tools to study bacteria. *Science (1979)* **346**, (2014).

40. Son, K., Brumley, D. R. & Stocker, R. Live from under the lens: exploring microbial motility with dynamic imaging and microfluidics. *Nat Rev Microbiol* **13**, 761–775 (2015).

41. Nagy, K., Ábrahám, Á., Keymer, J. E. & Galajda, P. Application of Microfluidics in Experimental Ecology: The Importance of Being Spatial. *Front Microbiol* **9**, (2018).

42. Borer, B., Tecon, R. & Or, D. Spatial organization of bacterial populations in response to oxygen and carbon counter-gradients in pore networks. *Nat Commun* **9**, (2018).

43. Weber, A., Bahrs, M., Alirezaeizanjani, Z., Zhang, X. & Beta, C. Rectification of Bacterial Diffusion in Microfluidic Labyrinths. *Front Phys* **7**, 1–11 (2019).

44. Rashid, S. *et al.* Adjustment in tumbling rates improves bacterial chemotaxis on obstacle-laden terrains. *Proceedings of the National Academy of Sciences* (2019) doi:10.1073/pnas.1816315116.

45. vande Broek, A., Lambrecht, M. & Vanderleyden, J. Bacterial chemotactic motility is important for the initiation of wheat root colonization by Azospirillum brasilense. *Microbiology (N Y)* **144**, 2599–2606 (1998).

46. Colin, R., Zhang, R. & Wilson, L. G. Fast, high-throughput measurement of collective behaviour in a bacterial population. *J R Soc Interface* **11**, 20140486–20140486 (2014).

47. Morse, M., Colin, R., Wilson, L. G. & Tang, J. X. The Aerotactic Response of Caulobacter crescentus. *Biophys J* **110**, 2076–2084 (2016).

48. Salek, M. M., Carrara, F., Fernandez, V., Guasto, J. S. & Stocker, R. Bacterial chemotaxis in a microfluidic T-maze reveals strong phenotypic heterogeneity in chemotactic sensitivity. *Nat Commun* (2019) doi:10.1038/s41467-019-09521-2.

49. Wu, Y., Park, H. B., Kai, T., Freeman, B. D. & Kalika, D. S. Water uptake , transport and structure characterization in poly (ethylene glycol) diacrylate hydrogels. *J Memb Sci* **347**, 197–208 (2010).

50. Yang, W., Yu, H., Liang, W., Wang, Y. & Liu, L. Rapid fabrication of hydrogel microstructures using UV-induced projection printing. *Micromachines (Basel)* **6**, 1903–1913 (2015).

51. Moffitt, J. R., Lee, J. B. & Cluzel, P. The single-cell chemostat: an agarose-based, microfluidic device for high-throughput, single-cell studies of bacteria and bacterial communities. *Lab Chip* **12**, 1487 (2012).

52. Roggo, C. *et al.* Quantitative chemical biosensing by bacterial chemotaxis in microfluidic chips. *Environ Microbiol* **20**, 241–258 (2018).

53. Moustafa, M. E. *et al.* Large area micropatterning of cells on polydimethylsiloxane surfaces. *J Biol Eng* **8**, 1–10 (2014).

54. Pratt, J. T., Tamayo, R., Tischler, A. D. & Camilli, A. PilZ domain proteins bind cyclic diguanylate and regulate diverse processes in Vibrio cholerae. *Journal of Biological Chemistry* **282**, 12860–12870 (2007).

55. Gumerov, V. M., Ortega, D. R., Adebali, O., Ulrich, L. E. & Zhulin, I. B. MiST 3 . 0 : an updated microbial signal transduction database with an emphasis on chemosensory systems SCHEMES. *Nucleic Acids Res* 1–6 (2019) doi:10.1093/nar/gkz988.

56. Bible, A. N., Stephens, B. B., Ortega, D. R., Xie, Z. & Alexandre, G. Function of a chemotaxis-like signal transduction pathway in modulating motility, cell clumping, and cell length in the alphaproteobacterium Azospirillum brasilense. *J Bacteriol* **190**, 6365–6375 (2008).

57. Müller, K., Naumann, S., Weber, W. & Zurbriggen, M. D. Optogenetics for gene expression in mammalian cells. *Biol Chem* **396**, 145–152 (2015).

58. Qin, D., Xia, Y. & Whitesides, G. M. Soft lithography for micro- and nanoscale patterning. *Nat Protoc* **5**, 491–502 (2010).

59. Traore, M. A. & Behkam, B. A PEG-DA microfluidic device for chemotaxis studies. *Journal of Micromechanics and Microengineering* **23**, (2013).

60. Cuchiara, M. P., Allen, A. C. B., Chen, T. M., Miller, J. S. & West, J. L. Multilayer microfluidic PEGDA hydrogels. *Biomaterials* **31**, 5491–5497 (2010).

61. Keenan, T. M. & Folch, A. Biomolecular gradients in cell culture systems. *Lab Chip* **8**, 34–57 (2008).

62. Blackburn, N., Fenchel, T. & Mitchell, J. *Microscale Nutrient Patches in Planktonic Habitats Shown by Chemotactic Bacteria*. *Behav. Neural Biol* vol. 57 (1992).

63. Jang, I., Kim, G. & Song, S. Mathematical model for mixing in a paper-based channel and applications to the generation of a concentration gradient. *Int J Heat Mass Transf* **120**, 830–837 (2018).

64. Singh, R. *et al.* Real rock-microfluidic flow cell: A test bed for real-time in situ analysis of flow, transport, and reaction in a subsurface reactive transport environment. *J Contam Hydrol* **204**, 28–39 (2017).

65. Walsh, E. J. *et al.* Microfluidics with fluid walls. *Nat Commun* **8**, (2017).

66. Wang, P. *et al.* Robust growth of escherichia coli. *Current Biology* **20**, 1099–1103 (2010).

67. Wang, S. J., Saadi, W., Lin, F., Minh-Canh Nguyen, C. & Li Jeon, N. Differential effects of EGF gradient profiles on MDA-MB-231 breast cancer cell chemotaxis. *Exp Cell Res* **300**, 180–189 (2004).

68. Lin, F. *et al.* Generation of dynamic temporal and spatial concentration gradients using microfluidic devices. *Lab Chip* **4**, 164 (2004).

69. Lin, F. *et al.* Effective neutrophil chemotaxis is strongly influenced by mean IL-8 concentration. *Biochem Biophys Res Commun* **319**, 576–581 (2004).

70. Saadi, W., Wang, S. J., Lin, F. & Jeon, N. L. A parallel-gradient microfluidic chamber for quantitative analysis of breast cancer cell chemotaxis. *Biomed Microdevices* **8**, 109–118 (2006).

71. Chung, B. G. *et al.* Human neural stem cell growth and differentiation in a gradient-generating microfluidic device. *Lab Chip* **5**, 401 (2005).

72. Linke, M., Köfinger, J. & Hummer, G. Fully Anisotropic Rotational Diffusion Tensor from Molecular Dynamics Simulations. *J Phys Chem B* **122**, 5630–5639 (2018).

73. Chaban, B., Hughes, H. V. & Beeby, M. The flagellum in bacterial pathogens: For motility and a whole lot more. *Seminars in Cell and Developmental Biology* vol. 46 91–103 Preprint at https://doi.org/10.1016/j.semcdb.2015.10.032 (2015).